



ISME

Friction-Stir-Processing Effect on Fracture Toughness of Oil Pipelines in ST 37 Group Before/After Nano ZrO₂-Coating

S. M. H. Sharifi*
Assistant Professor

A. Sabetghadam-
Isfahani†
MSc. Student

Y. Davoodbeygi‡
Ph.D Candidate

Herein, Compact Testing (CT) and Charpy V-Notch (CVN) testing have been done on four Friction-Stir-Processed (FSPed) samples: BM (Base-Metal), FS (FSPed-Sample), FN5 (FSP Nano-ZrO₂-coated/560 rpm rotational speed) and FN9 (FSP Nano-ZrO₂-coated/900 rpm), to investigate the K_{IC} and the dominant parameters on it for St 37 steel. Experiments are also surveyed and validated by ABAQUS. Results showed the greatest K_{IC} value for BM (CT: 110.40 /CVN: 98.72 MPa√m) and the least for FN9 (CT: 72.20/CVN: 60.08 MPa√m). FSP caused brittle behavior but not as much as FSP Nano-coating. The calculation of CT samples was done in Gerson theory by using of LEFM (Linear Elastic Fracture Mechanics) formulas. Investigations showed more reliability for CVN obtained results. The K_{IC} and ductile fracture decreased after FSP for both CVN and CT.

Keywords: K_{IC} , CVN, CT, Crack Propagation, FSP Nano-coating.

1 Introduction

Gas and oil, together, provide more than 68% of whole world energy [1]. This energy is transported from the production source to the consumption units by means of pipelines. In last century, all tries were concentrated on promoting oil and gas industry to transport them in high pressure and getting better performance. Doing this is owe to use pipelines with bigger diameter and less thickness due to minimize the cost of pipelines per meter. These structures are designed to tolerate an inner pressure in about 10-15 (MPa) which is about 75-80% of minimum nominal stress of steel [2]. In this situation, safety and having no defects of the structure and its resistance against ductile crack propagation has a great importance in the view of pipelines engineer designers. These crack propagations can be because of corrosion, welding defects, impact, fatigue and etc. So finding a method to change the ductile crack propagation to brittle crack propagation seems necessary [3]. To increase the steel strength against crack propagation, a controlled thermal process with micro alloys is used. Because of impurity in matrix of steel, some defects as holes appears in the material which decreases its strength.

*Assistant Professor, Department of Mechanical Engineering, Petroleum University of Technology, Ahvaz Faculty, Iran

†Corresponding Author, MSc. , Department of Mechanical Engineering, Petroleum University of Technology, Ahvaz Faculty, Iran arminsabet1990@gmail.com

‡ Ph.D Student, Department of Chemical Engineering, Faculty of Engineering, University of Kashan, Kashan, Iran

These defects are the main reasons of fracture in ductile materials and ductile fracture is a main reason of tearing in engineering structures [4]. Crack propagation in ductile materials (in first mode) in tension includes three steps of initiation, propagation and mixing of microstructure holes caused by Mn sulfide and Fe carbide. Inversely, crack propagation in brittle materials because of material's high thickness, low temperature and high loading rate occurs in form of intergranular and transgranular [5].

Recently, a new processing technique, FSP, was developed by Mishra et al., [6,7] for microstructural modification based on the basic principles of FSW. In this case, a rotating tool with pin and shoulder is inserted in a single piece of material, for localized microstructural modification for specific property enhancement. For example, a fine-grained microstructure for high-strain-rate superplasticity was obtained in the commercial 7075Al alloy through FSP [6,8]. Furthermore, the FSP technique has been used for the fabrication of a surface composite on aluminum substrate, [9] and the homogenization of powder metallurgy aluminum alloys, metal matrix composites, and cast aluminum alloys [10-12].

Compared to other metalworking techniques, FSP has distinct advantages [6-9]. First, FSP is a short-route, solid-state processing technique with one-step processing that achieves microstructural refinement, densification, and homogeneity [13]. Second, the microstructure and mechanical properties of the processed zone can be accurately controlled by optimizing the tool design, FSP parameters, and active cooling/heating [14]. Third, the depth of the processed zone can be optionally adjusted by changing the length of the tool pin, with the depth being between several hundred micrometers and tens of millimeters [15, 16].

Fourth, FSP is a versatile technique with a comprehensive function for the fabrication, processing, and synthesis of materials [17]. Fifth, the heat input during FSP comes from friction and plastic deformation, which means FSP is a green and energy-efficient technique without deleterious gas, irradiation, and noise [18]. Sixth, FSP does not change the shape and size of the processed components [19]. The FSP technique is emerging as a very effective solid-state processing technique that can provide localized modification and control of microstructures in the near-surface layers of processed metallic components [20, 21]. In the relatively short duration after its invention, increasing applications are being found for FSP in the fabrication, processing, and synthesis of metallic materials [22-24].

Fracture toughness shows the capability of the material in brittle fracture. Since existence of a crack or its propagation in a pipeline is so dangerous and can cause lots of destructions, so strong designing against crack and crack propagation is so important. The strength of the used materials in pipelines must be in such quality when cracks initiate in the pipelines, materials resistant against crack propagation. This matter holds the importance of finding fracture toughness in pipelines. The role of FSP on promoting metals resistance against ductile crack propagation and change it to brittle crack propagation is noticeable [25].

Herein, according to some restrictions on providing K_{IC} samples (refers to thickness), an indirect method was used in which from obtaining J_{IC} , K_{IC} was obtained. To make K_{IC} samples, a thickness about 40 cm is needed which does not exist for the used pipelines, so J_{IC} samples are used to obtain the value of K_{IC} [26]. Lendes and Begley were the first persons who calculated J from definition of released energy rate. They made samples with different geometric dimensions and crack length but the same material. All samples were put under loading and then force-strike curve was extracted for all of them. The below area of each curve showed the attracted energy (showed by U) by the sample. The curve of strike-crack length stretched in constant displacement [27]. Another method of obtaining K_{IC} is Charpy impact test. Jong an et al, found fracture toughness of API X65 pipelines' steel [28]. They did their experiments in range temperature of -40 to 20 °C with pre-strain rates (from 0% up to 10%). The obtained value of K_{IC} in ambient temperature was about 98.72 $\text{Mpa}\sqrt{\text{m}}$.

2 Experiments

2.1 Chemical Composition

A 25.4 mm by 25.4 mm sample was sectioned from a corner of the plate using a Struers Sectom-10 diamond saw. This sample was sent for chemical analysis at Metallurgy Laboratory of Sharif Jahad, to determine the chemical composition of the steel used in this work. Table (1) gives the composition limits for St 37 steel according to MIL-S-16216K [29]. Chemical composition and mechanical properties of BM are presented in Table (1) and (2), respectively.

2.2 K_{IC} Tests Sample Preparation

The experimented samples are CT and CVN with geometric shapes according to Figure (1). CT sample's width is 10 and thickness 15 mm. But CVN samples were prepared in subsize form. The BM of samples is St 37 steel. Figure (2) shows the CT test apparatus. Some of CT and CVN samples are shown in Figure (3). To find K_{IC} from CT, ASTM E 399-09 standard was used. Since the used specimens had thickness restrictions, so static fracture toughness test was not able to be done. Instead the ASTM STP 514 Part 2 standard was used. The CVN samples were made and done according to ASTM E23.

Table 1 Chemical composition of the St 37 steel.

St 37	Fe	C	Si	Mn	P	S	Cr	Ni	Mo	Al
Weight Percent	Base	0.131	0.0657	0.445	0.0092	0.0207	0.0278	0.0286	0.0023	0.0403
St 37	Co	Cu	Nb	Ti	V	W	Pb	Sn	As	Zr
Weight Percent	0.0045	0.0616	0.00072	0.00046	0.0023	0.0049	0.0023	0.0043	0.0029	0.00054

Table 2 Mechanical properties of St 37 steel.

	Yield Stress (MPa)	Young Modulus (GPa)	Poisson Ratio
Before FSP	210	105	0.3
After FSP	250	125	0.3

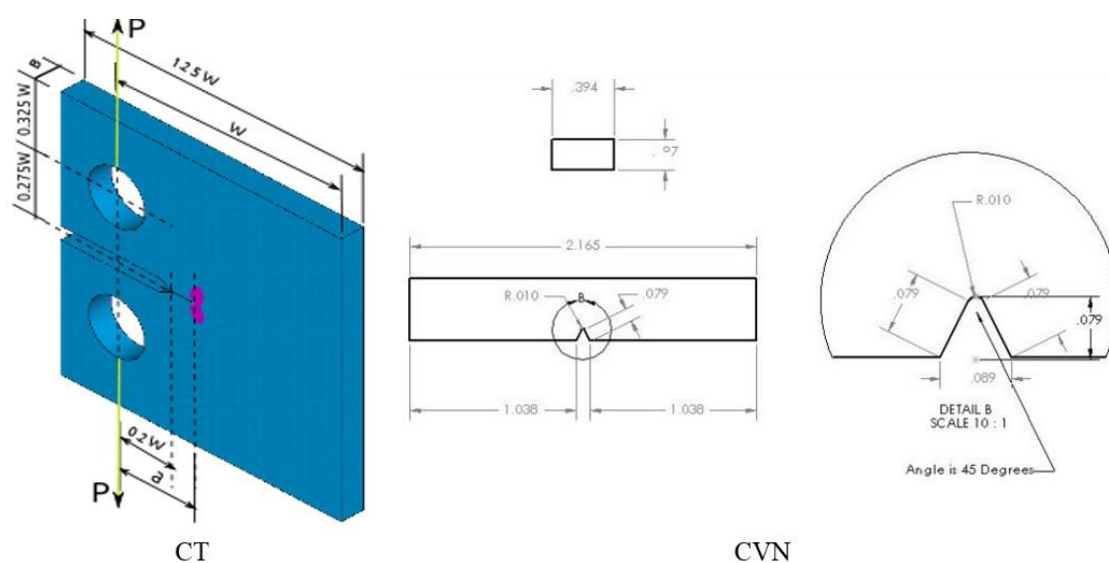


Figure 1 Dimensions of CT and CVN test sample.



Figure 2 CT test apparatus.

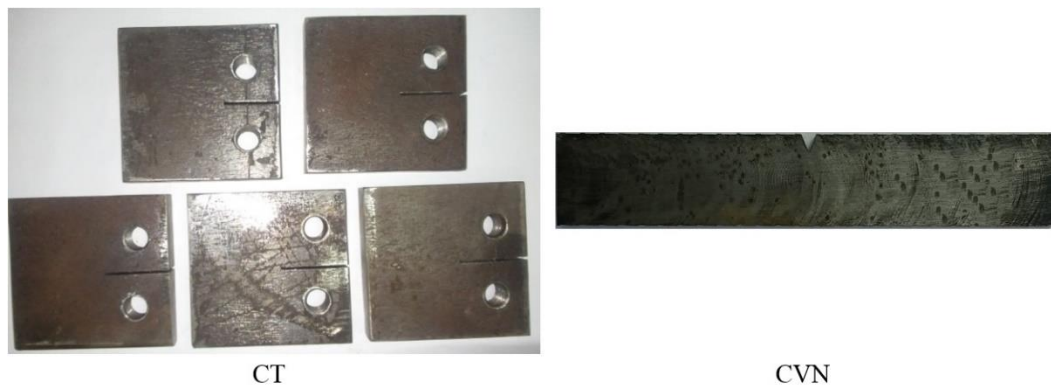


Figure 3 Some of CT samples.

Table 3 Test temperatures of Charpy V-Notch samples.

Dry FSP Samples	
Temperature	Solution
Room Temp	Ice and Salt Water (NaCl)

2.3 Charpy V-Notch Testing

Three each Charpy V-Notch samples (before and after FSP) were chilled for five minutes at a room temperatures shown in Table (3). Temperatures were obtained by mixing ice, salt, water together in varying amounts in an insulated container. Samples were quickly transferred from baths to Charpy Impact Energy tester and broken. Samples were removed and washed with methanol to preserve the fracture surface for future fractography examination.

If temperature is chosen as the parameter to correlate in the K_{IC} test, it also has to be chosen in the Charpy V-Notch test. The chosen temperature must, in addition to fulfilling the same requirements as in the case of K_{IC} correspond to a low enough energy so that the impact energy value will not depend on the applied testing standard. Also, because ductile crack growth is not allowed, a temperature corresponding close to the lower shelf must be chosen. On the other hand, the chosen temperature should correspond to the increasing part of the transition curve and it is also recommendable to choose a commonly recognized energy-level. One such temperature is the transition temperature corresponding to Charpy V-Notch impact energy 28 J. This temperature is also equivalent to the temperature used by Marandet and Sanz [30] in their empirical correlation which did not consider the effects of the test differences theoretically.

The chosen impact energy level is practically independent of testing standards and at this energy level the amount of ductile tearing is small. Remaining, strongly affecting, factors are the effect of the blunt notch and the effect of loading rate difference. An increasing loading rate shifts the toughness transition to higher temperatures and the magnitude of the effect is inversely related to the materials yield strength. Based on the theoretical treatment, the temperatures TK_{28J} and $TK_{100MPa\sqrt{m}}$ were selected for correlation [31,32]. Results from 141 materials fulfilling the requirements were analyzed. The correlation has the form [33]:

$$TK_{100MPa\sqrt{m}} = TK_{28J} - 18^{\circ}C \quad (1)$$

Finally, guidelines to determine the fracture toughness from impact test results has been presented. The fracture toughness can be expressed as a function of the Charpy-V transition temperature [33]:

$$K_{IC} = 20 + \left(11 + 77 \cdot \exp\left(0.019 \cdot (T - TK_{28J} + 18^{\circ}C)\right)\right) \cdot \left(\frac{25}{B}\right)^{1/4} \cdot \left(\ln \frac{1}{1 - P_f}\right)^{1/4} \quad (2)$$

Where TK_{28J} includes the correlation scatter and has the standard deviation $13^{\circ}C$. P_f is calculated from Equation (3):

$$P_f = 1 - \exp\left(-\left(\frac{K_1 - K_{min}}{K_0 - K_{min}}\right)^4\right) \quad (3)$$

Where P_f is the cumulative failure probability at a stress intensity factor level, K_1 and K_0 is a specimen thickness and temperature dependent normalization parameter. The temperature dependence of K_0 in $MPa\sqrt{m}$ can successfully be described with [34]:

$$K_0 = \alpha + \beta \cdot \exp(\gamma \cdot (T - T_0)) \quad (4)$$

Where $\alpha + \beta = 108 MPa\sqrt{m}$, T_0 is the temperature (in $^{\circ}C$) at which the mean fracture toughness is $100 MPa\sqrt{m}$ and γ is a material constant. K_{min} is the lower bound fracture toughness which for steels is close to $20 MPa\sqrt{m}$.

Transition in K_{IC} or CVN values for steels usually takes place below room temperatures. For tool steels used in cold working or in sub-zero atmospheres, a K_{IC} prediction strategy based on the transition temperature approach could thus be quite suitable by Marandet and Sanz [34], employed a multi-step approach to predict a K_{IC} -temperature curve for a set of medium-strength steels having various heat treatments. By taking K_{IC} transition-temperature (TK^*_{IC}) as the temperature at which toughness increases rapidly, they defined TK^*_{IC} as the temperature for which $K^*_{IC} = 100 MPa\sqrt{m}$. Similarly, they defined TK_{28} as the impact transition temperature, the temperature at which Charpy V-Notch energy is $CVN = 28 J$. By observing the transition trends for the steels studied, they suggested the relationship [34]:

$$TK^*_{IC} = 9 + 1.37TK_{28} \text{ (}^{\circ}C\text{)} \quad (5)$$

They also determined that by shifting the actual K_{IC} -temperature curves until TK^*_{IC} coincided with TK_{28} , a K_{IC} -CVN correlation can be established as [35]:

$$K_{IC} = 19(CVN)^{1/2} \quad (6)$$

2.4 J-Integral Method of CT

According to ASTM STP 514 Part 2 standard [35], dynamic fracture toughness test was done. The first step is to generate a J resistance curve. To ensure that the crack front is straight the use of a side grooved specimen is recommended.

A series of nominally identical specimens are loaded to various level and then unloaded. The crack growth in each sample, which will be different is carefully marked by heat tinting or fatigue cracking after the test. The load-displacement curve for each sample is recorded. Each specimen broken open and the crack growth in each specimen is measured. J is divided into elastic and plastic components, and these two parts will be calculated by using 7-10 formulas. After extracting the force-displacement curve; the below curve area from zero point to the first maximum is calculated. By replacing it in Equation (7) the elastic part of the J-Integral is found:

$$J_{el} = \frac{(2 \times A)}{(L \times B)} \quad (7)$$

Where A is the mentioned area, L is the ligament (W-a), “W” and “a” are shown in Figure (1) and B is the thickness. After finding J_{el} , K_{IC} is calculated from Equation (8):

$$J_{el} = (K_{IC})^2 \frac{(1 - \nu^2)}{E} \quad (8)$$

J_{pl} is obtained from (9) and (10) formulas:

$$J_{pl} = \frac{\eta A_{pl}}{BL} \quad (9)$$

$$\eta = 2 + 0.522(L/W) \quad (10)$$

The force-displacement curve of dynamic fracture toughness test is shown in Figure (4). It must be mentioned that since K_{IC} is important to be found, so only J_{el} has been calculated. The below curve area is calculated by “ARIAN AREA FINDER” software and then K_{IC} is calculated from Equation (7) and (8). Dynamic fracture toughness test was repeating three times before and after FSP. Totally six dynamic fracture toughness tests were done. The calculated area and the obtained J-Integral is shown in Table (4).

Table 4 Below load-displacement curves' area and the calculated J-Integrals.

Samples Code	BM (Base Metal)	FS	FN9
Area	83.81	63.92	44.71
J-Integral (MJ)	44.37	44.28	1.39

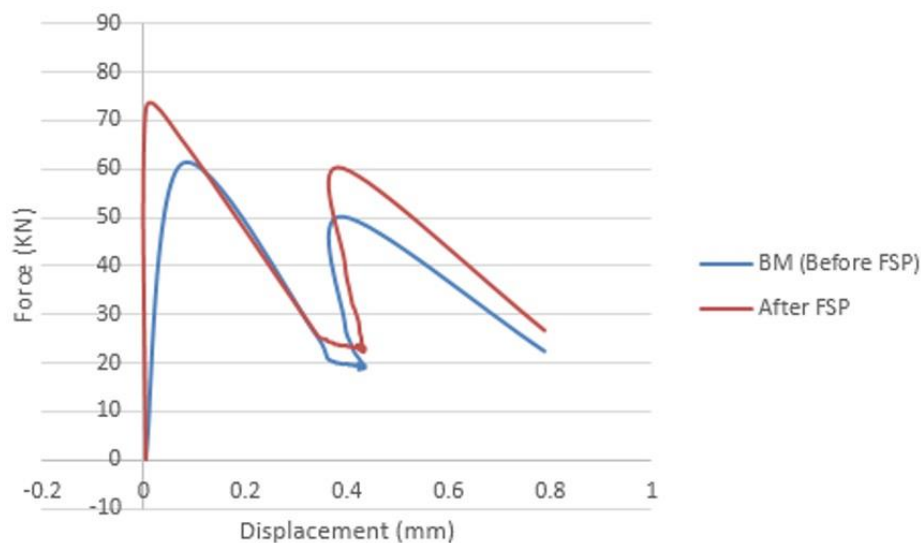


Figure 4 Dynamic fracture toughness load-displacement curve.

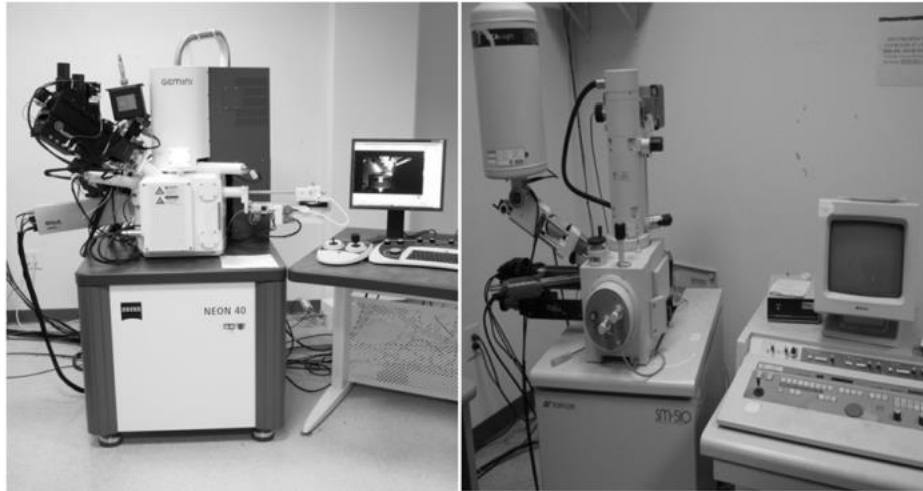


Figure 5 (Left) SEM Zeiss Neon 40 (Right) JFC-1100.

2-5 SEM Specification

High resolution imaging was conducted using the Sharif University of Technology's Ion Sputter JFC-1100 scanning electron microscope that is equipped with field emission filament. However, half-way through the study the JFC SEM had a mechanical failure and the samples were further analyzed using Razi's Ziess SEM with a LaB6 filament, Figure (5).

Both microscopes imaged the samples at an accelerating voltage of 15 KeV or 20 KeV with a working distance of around 5 mm (Zeiss) or 22 mm (JFC).

3 Simulation

All samples' simulations before and after FSP are done in ABAQUS software. For simulating, mechanical properties are imported from Table (2) and other needed mechanical properties are imported from standards [36].

In Figure (6) a view of simulation is shown. In simulation, CT test sample is simulated according to real dimensions and the same loading condition. It must be mentioned, since in simulations the optimal elements and mesh of various parts are different; the elements far away the crack tip, have rectangular shape and the elements near the crack tip, have triangular or irregular 4-sides (cohesive to the crack tip) shapes.

So first, simulation was done in static loading with great meshes and then smoothly they were decreased to reach the optimised size of each mentioned elements' shape. The goal of using static loading is to find the optimile size of elements after finding them the simulation must be done in experiment situation that is dynamic loading. At the end, it must be mentioned that obtained optimized elements has been used for simulating and the simulation is done in PSN state. Mesh dimension near crack were considered about 0.2 mm [37, 38, 39].

Another point in case of simulation is the differences of experiments' and simulations' results; the reason why these defferences has occured is exactly goes to the simulation restrictions. In ABAQUS there is no ability to simulate 3D crack propagation; so a great difference is emerging between the experiments' and simulations' results.

In Figure (7), the simulated sample is shown after dynamic loading. In simulation damage Gerson model has been used. To use this model, first, its coefficients must be obtained from tension test and imported to the software.

This theory has some constants for every metal and for the used metal in this research (St 37) are mentioned in Table 5 [36]. These coefficients are the average elongation of dimples' stick, deviation of dimples' distribution standard, volume fraction for dimples' stick, initial volume fraction of dimples, critical value (volume fraction in merging dimples initiation), fraction volume of dimple in fracture point, and two final coefficients are regular makers in yeilding function. This model is usually considered in finite element software products as Gerson-Tvergaard-Needleman or GTN model. For simulating in ABAQUS, GTN damage model has been used which contains all these 8 parameters and makes the simulation much easier [40].

4 Results and Discussion

4.1 Charpy V-Notch Testing

The obtained results of Charpy V-Notch test is shown in Table (6) and the extracted K_{IC} is shown in Table (7). As it is clear from the CVN tests' obtaind results, after FSP, K_{IC} magnitude is decreased and it shows the changing behavior of St 37 metal to have more brittle characteristics. This brittle behavior increases by FSP Nano ZrO_2 -coating.

The results show using Nano particles during the FSP will increase the brittle behavior in matals and also doing FSP in high rotational speed will cause more brittle behavior in comparision to low ones. The mentioned goal of this paper was decreasing K_{IC} magnitude.

It is noticeable that having more brittle behaviour, causes more yeilding, ultimate and fracture strength, but the less elongation. So according to this matter, metals with brittle behaviour are so good and appropriate to be used in regions that have corrosion and erosion maker enviroments or for the some usages that metals are needed to sustain high rate of tension, pressure or fatigue loading [26].

Table 5 Constants of Gerson theory for St 37.

Parameter	Value
q_1	1.5
q_2	1
ϵ_N	0.3
S_N	0.1
f_N	0.003
f_0	7.07×10^{-5}
f_c	0.019
f_f	0.29

Table 6 Charpy v-notched results for the samples.

Sample Code	Temperature (°C)	Charpy V-Notched Energy (J)
BM	20	27
FS	20	18
FN5	20	12
FN9	20	10

Table 7 Fracture toughness of all samples, obtained from CVN.

Sample Code	K_{IC} (MPa \sqrt{m})	CVN magnitude (J)
BM	98.72	27
FS	80.61	18
FN5	65.36	12
FN9	60.08	10

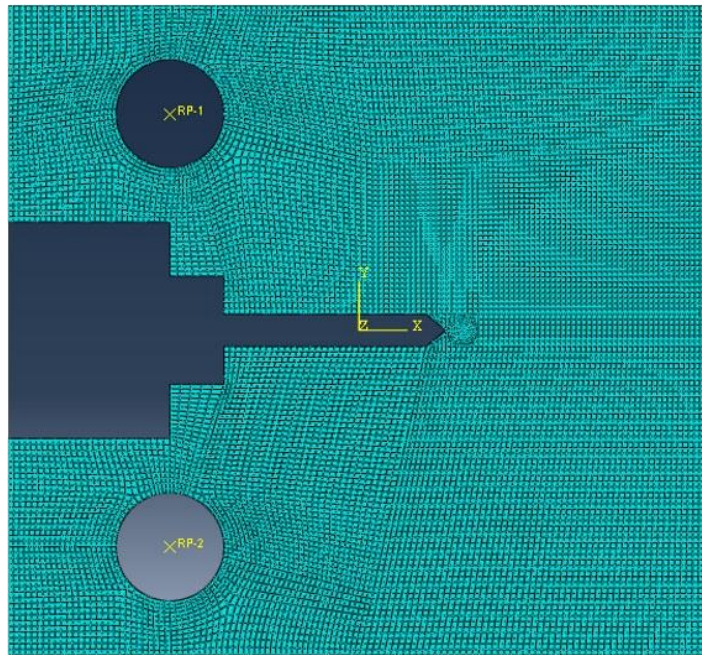


Figure 6 Simulated CT test sample.

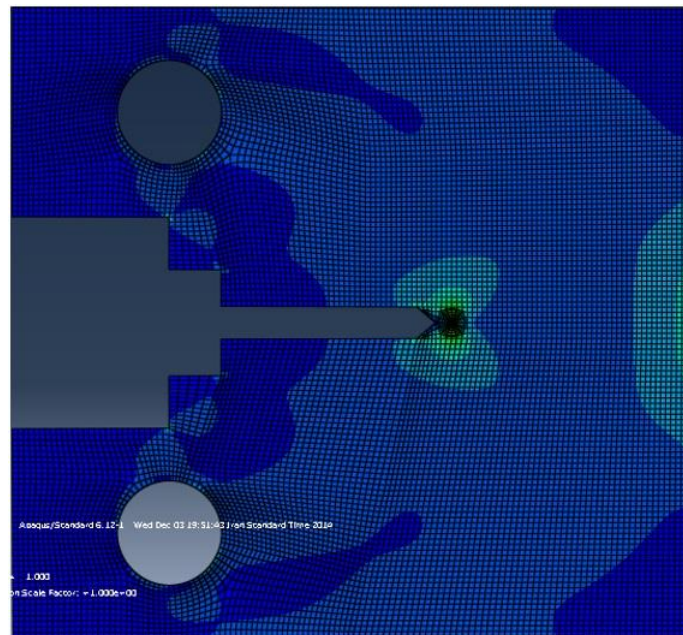


Figure 7 Simulated CT test after dynamic loading.

4.2 Fractography

The fracture surface of the CT (for FS and FN9 samples) at room temperature, is shown in Figure (8). The fracture surface is the most important case in all fracture SEMs, since it shows the kind of fracture (brittle or ductile). The smooth fracture surface shows a brittle fracture and the serrated one shows a ductile fracture. As it is seen in Figure (8), the smoothest fracture surface is for FN9 sample which shows it is the hardest sample and the most serrated one is for FS which has the least hardness among three mentioned samples. All part's results are covering and are in good agreement with each other.

As it is clear, crack initiation and propagation are essential for the fracture happening. The manner through which the crack propagates through the material gives great insight into the mode of fracture. In ductile materials (ductile fracture), the crack moves slowly and is accompanied by a large amount of plastic deformation. The crack will usually not extend unless an increased stress is applied. On the other hand, in dealing with brittle fracture, cracks spread very rapidly with little or no plastic deformation. The cracks that propagate in a brittle material will continue to grow and increase in magnitude once they are initiated. Another important mannerism of crack propagation is the way in which the advancing crack travels through the material. A crack that passes through the grains within the materials is undergoing transgranular fracture. However, a crack that propagates along the grain boundaries is termed an intergranular fracture. On both macroscopic and microscopic levels, ductile fracture surfaces have distinct features. Macroscopically, ductile fracture surfaces have larger necking regions and an overall rougher appearance than a brittle fracture surface. On the microscopic level, ductile fracture surfaces also appear rough and irregular. The surface consists of many microvoids and dimples. In Figure (9), microvoids and dimple sizes of FS, FN5 and FN9 samples are shown.

As it is clear after FSP, dimple sizes decreased and it shows more brittle behavior of the metal. By adding Nano ZrO_2 the dimple sizes are decreasing more and by increasing the rotational speed more decrease in dimple sizes occurred. So totally, the FN9 sample which had the highest rotational speed and was coated by Nano ZrO_2 experienced the most decrease in its dimple sizes and the FFS sample experienced the least. Decrease of dimple sizes is related to decrease of plastic zone radiation and consequently happening of soft fracture surface [39]. Another reason of dimple sizes' decrease after FSP is related to ZENER pinning effect. ZENER pinning is the influence of a disoersion of fine particles on the movement of low-and high angle grain boundaries through a polycrystalline material [39].

Small particles act to prevent the motion of such boundaries by exerting a pinning pressure which counteracts the driving force pushing the boundaries. ZENER pinning effect is very important in materials processing as it has a strong influence on recovery, recrystallization and grain growth [39]. According to ZENER pinning effect, during FSP, grain boundaries break and recrystelize more regular and smaller; simeltaneusely, particles sit on boundaries and prevent from grains' size inhance. So these new grains in fracture show more brittle behavior and logically the fracture happens fast and soft, which all will cause smaller dimple sizes. Exactlly this trend of recrystallization is true about adding Nano particles and increasing the rotational speed [39].

4.3 CT Method

According to Figure (4), as it is clear by moving to brittle samples, maximum load increases and occurs in less displacements, so below curve area decreases. It is a reasonable result and confirms, totally, all CVN tests and SEM analysis. By mentioned method in Part 2.4, the magnitude of J-Integral was found for all samples. The below area of load-displacement curves in its first maximum load was found bay "ARIAN AREA CALCULATOR" software. This software is an exact software used in curves area calculation. Obtained area from curves and the calculated J-Integral from them are shown in Table (8).

The magnitude of K_{IC} for all samples is calculated and presented in Table (9). As it is clear, order of CVN results are true about the fracture toughness test. Certainly, There is some mismatches between CVN and dynamic fracture toughness test which are compared in Table (10). It seems that CVN results are more reliable, since, during the experiments, no defect seen but in fracture toughness tests lots of defects consist of human defects and errors, apparatus errors and new used method could affect the results [41]. Totally, the range of magnitudes are the same but they are not exactly the same. It is prefered to use CVN to detect K_{IC} ($MPa\sqrt{m}$).

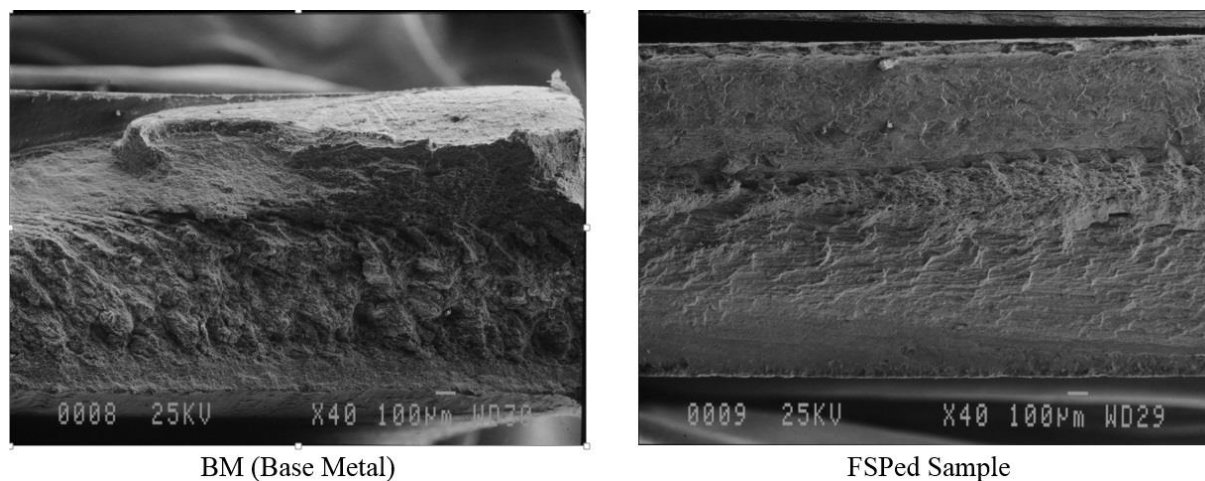


Figure 8 Fracture surface SEMs of FS and FS9 samples.

Table 8 Below load-displacement curves' area and the calculated J-Integrals.

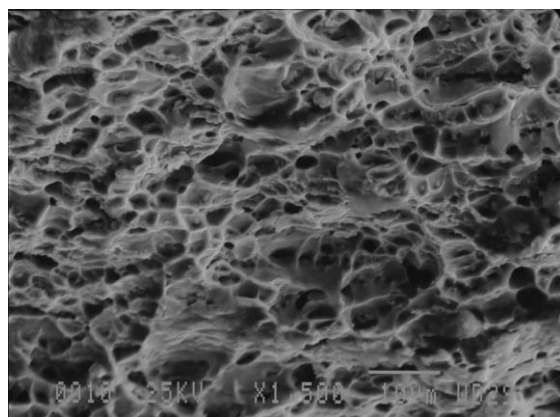
Samples Code	BM	FN5	FN9	FS
Area	83.81	53.26	44.71	63.92
J-Integral (MJ)	44.37	16.47	1.39	44.28

Table 9 Magnitude of K_{IC} for all samples.

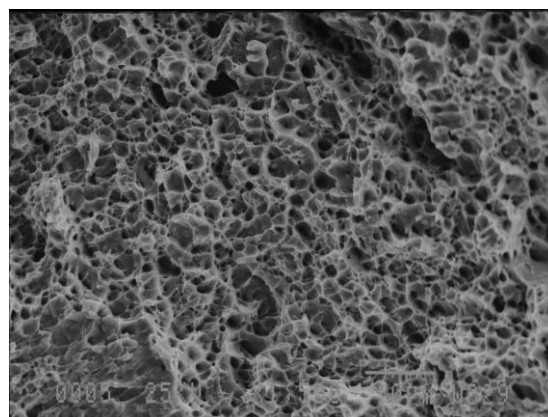
Samples Code	BM	FN5	FN9	FS
K_{IC} (MPa \sqrt{m})	110.4	75.6	72.2	101.7

Table 10 Comparison of CVN, dynamic fracture toughness and simulation results.

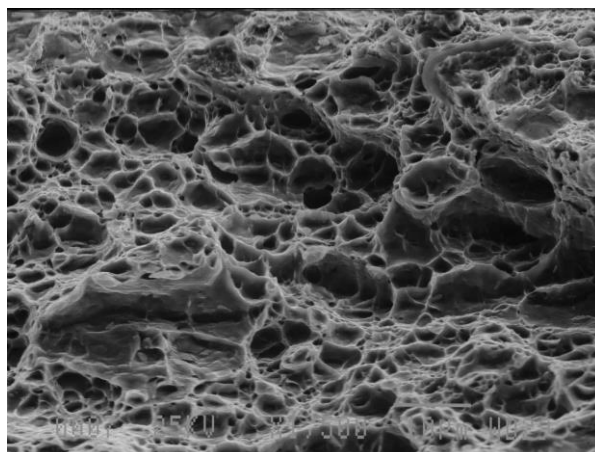
Samples Code	BM	FN5	FN9	FS
Fracture toughness test	110.4	75.6	72.2	101.7
CVN	98.72	65.36	60.08	80.61
Simulation	120	98.5	97	115.3
% (CVN/Fractour Toughness Test)	10.57	13.54	16.70	20.73
% (Simulation/Fracture Toughness)	8.00	22.67	25.56	11.79



(a)



(b)



(c)

Figure 9 Microvoids and dimple sizes of fracture surface; a) FN5 b) FN9 c) FS.

5 Conclusion

In this work; first, Friction stir processing was conducted on St 37 in dry form; second, moreover of FSP, Nano ZrO_2 -coating was done on it; and third, the rotational speed of Nano coating was increased from 560 rpm to 900 rpm. These processes were then sectioned, examined microscopically, mechanically tested and finally simulated by ABAQUS software. These results were then compared to non FSP treated base metal to determine if FSP and Nano-coating were feasible. Furthermore, the effect of CVN and CT on obtaining K_{IC} was surveyed too. The following conclusions were demonstrated:

- Deformation during FSP of St 37 did not result in the elongation of the grains in out of FSPed region..
- The grain sizes and dimmple sizes (produced holes after farcture) have the smallest value for FN9 and then FN5, FS and BM, respectively.
- The value of K_{IC} (Fracture toughness magnitude of the metal) is declining in order of BS, FS, FN5 and FN9 in both CVN and CT methods, how the FN9 sample has the lowest magnitude.
- Exactness of CVN method for obtaining K_{IC} is quite more than CT method probably sice its results are obtaining by doing more repeatitive experiments.

Finally, it can be concluded that for obtaining K_{IC} (fracture toughness) of metals with high yeilding strength in which PSN (Plain Strain State) does not happen, CVN (Charpy V-Notch Testing) method is more exact in comparison to CT (Compact Test) method.

Furthermore, after doing FSP, base metal finds more brittle behavior, meanwhile, this brittle behavior by Nano ZrO_2 -coating and rotational speed increase will br fortified more. The more brittle behavior of materials more decrease or prevention of ductile fracture, according to the usage type of base metal this feature can considered as an advantage.

For observed pipelines in this paper (pipelines in St 37 group), this feature observed as an advantage. Since their vital fracture's roots characteristics are dependant to impact in high rate elongation, erosion and corrosion which all are more perilous in ductile form not in brittle.

References

- [1] Aktarer, S. M., Sekban, D. M., Saray, O., and Kucukomero, T., “Effect of Two-pass Friction Stir Processing on the Microstructure and Mechanical Properties of As-cast Binary Al–12Si Alloy”, *Materials Science and Engineering*, Vol. 636, pp. 311-319, (2015).
- [2] Anon, A., “*Measure of Fracture Toughness E813-89*”, 1st Edition, Annual Book of ASTM Standards, New York, pp. 241, (1991).
- [3] Beak, J. H., Kim, Y. P., Kim, C. M., and Seo, W. S., “Effect of Pre-strain on the Mechanical Properties of API X65 Pipe”, *Material and Science*, Vol. 30, pp. 1473-1479, (2010).
- [4] Miehe, C., “Phase Field Modeling of Fracture in Multi-physics Problems”, *Computer Methods in Applied Mechanics and Engineering*, Vol. 42, pp. 163-172, (2014).
- [5] Cui, L., “Friction Stir Welding of a High Carbon Steel”, *Scripta Materialia*, Vol. 56, pp. 637-638, (2007).
- [6] Mishra, R. S., Mahoney, M. W., McFadden, S. X., Mara, N. A., and Mukherjee, A. K., “High Strain Rate Superplasticity in a Friction Stir Processed 7075 Al Alloy”, *Scripta Materialia*, Vol. 42, pp. 163–168, (2000).
- [7] Mishra, R. S., and Mahoney, M. W., “Low Temperature Superplasticity in a Friction-stir-processed Ultrafine Grained Al–Zn–Mg–Sc Alloy”, *Materials Science Forum*, Vols. 357–359, pp. 507–12, (2001).
- [8] Ma, Z. Y., Mishra, R. S., and Mahoney, M. W., “Effect of Friction Stir Processing on the Kinetics of Superplastic Deformation in an Al-Mg-Zr Alloy”, *Acta Materialia*, Vol. 50, pp. 4419–4430, (2002).
- [9] Mishra, R. S., Ma, Z. Y., and Charit, I., “High Strain Rate Superplasticity in a Commercial 2024 Al Alloy via Friction Stir Processing”, *Materials Science and Engineering A*, Vol. A341, pp. 307–310, (2002).
- [10] Berbon, P. B., Bingel, W. H., Mishra, R. S., Bampton, C. C., and Mahoney, M. W., “Surface Hardening of Two Cast Irons by Friction Stir Processing”, *Scripta Materialia*, Vol. 44, pp. 61–66, (2001).
- [11] Spowart, J. E., Ma, Z. Y., and Mishra, R. S., “Superplastic Deformation Behaviour of Friction Stir Processed 7075Al Alloy”, *Friction Stir Welding and Processing II*, Vol. 12, pp. 243–252, (2003).
- [12] Ma, Z. Y., Sharma, S. R., Mishra, R. S., and Mahoney, M. W., “High Strain Rate Superplasticity in a Friction Stir Processed 7075 Al Alloy”, *Materials Science Forum*, Vol. 426-432, pp. 2891–2896, (2003).
- [13] Lee, C. J., Huang, J. C., and Hsieh, P. J., “Mg Based Nano-composites Fabricated by Friction Stir Processing”, *Scripta Materialia*, Vol. 54, pp. 1415–1420, (2006).
- [14] Morisada, Y., Fujii, H., Nagaoka, T., and Fukusumi, M., “Microstructural Investigation

- of Friction Stir Welded 7050-T651 Aluminium”, *Materials Science Engineering A*, Vol. A419, pp. 344–348, (2006).
- [15] Morisada, Y., Fujii, H., Nagaoka, T., and Fukusumi, M., “Effect of Friction Stir Processing with SiC Particles on Microstructure and Hardness of AZ31”, *Materials Science and Engineering A*, Vol. A433, pp. 50–54, (2006).
- [16] Dixit, M., Newkirk, J. W., and Mishra, R. S., “Properties of Friction Stir-processed Al 1100–NiTi Composite”, *Scripta Materialia*, Vol. 56, pp. 541–544, (2007).
- [17] Sharma, S. R., Ma, Z. Y., Mishra, R. S., and Mahoney, M. W., “Microstructural Modification of As-cast Al-Si-Mg Alloy by Friction Stir Processing”, *Scripta Materialia*, Vol. 51, pp. 237–241, (2004).
- [18] Ma, Z. Y., Sharma, S. R., Mishra, R. S., and Mahoney, M. W., “Friction Stir Processing of SSM356 Aluminium Alloy”, *Metallurgical and Materials Transactions A*, Vol. 37A, pp. 3323–3336, (2006).
- [19] Ma, Z. Y., Sharma, S. R., and Mishra, R. S., “Effect of Friction Stir Processing on Fatigue Behavior of A356 Alloy”, *Scripta Materialia*, Vol. 54, pp. 1623–1626, (2006).
- [20] Oh-ishi, K., and McNelley, T. R., “Effect of Friction Stir Processing Procedures on Microstructure and Mechanical Properties of Mg-Al-Zn Casting”, *Metallurgical and Materials Transactions A*, Vol. 35A, pp. 2951–2961, (2004).
- [21] Feng, A. H., and Ma, Z. Y., “Inhomogeneous Microstructure and Mechanical Properties of Friction Stir Processed As-cast NiAl Bronze”, *Scripta Materialia*, Vol. 56, pp. 397–400, (2007).
- [22] Hsu, C. J., Kao, P. W., and Ho, N. J., “Particle-reinforced Aluminum Matrix Composites Produced from Powder Mixtures Via Friction Stir Processing”, *Scripta Materialia*, Vol. 53, pp. 341–345, (2005).
- [23] Chuang, C. H., Huang, J. C., and Hsieh, P. J., “Using Friction Stir Processing to Fabricate MgAlZn Intermetallic Alloys”, *Scripta Materialia*, Vol. 53, pp. 1455–1460, (2005).
- [24] Hsu, C. J., Chang, C. Y., Kao, P. W., Ho, N. J., and Chang, C. P., “Al–Al₃Ti Nanocomposites Produced in Situ by Friction Stir Processing”, *Acta Materialia*, Vol. 54, pp. 5241–5249, (2006).
- [25] Daghyani, H., and Khodayee, F., “Introductory to Fracture Mechanics of Materials”, M. Sc. Thesis, Department of Mechanical Engineering, Amirkabir University of Technology, Tehran, (1379).
- [26] Hashemi, S. H., Rezaei, M., and Soleimani, V., “Local Damage Modeling of Ductile Fracture in API Pipeline Steels of Grade X65 and X70”, *Proceeding of ISME2011*, Vol. 2, pp. 44–52, (2011).
- [27] Hulka, K., “High Strength Large Diameter Pipe”, <http://www.us.cbmm.com.br/english/sources/techlib/info>. [Online], (2006).

- [28] Hütter, G., Mühlich, U., and Kuna, M., “Simulation of Local Instabilities During Crack Propagation in the Ductile–brittle Transition Region”, *Computer Methods in Applied Mechanics and Engineering*, Vol. 23, pp. 141-156, (2014).
- [29] Hyunmin, K., Minju, K., Hyeok, J. J., and Hyung, S., “Mechanisms of Toughness Improvement in Charpy Impact and Fracture Toughness Tests of Non-heat-treating Cold-drawn Steel Bar”, *Materials Science and Engineering*, Vol. 571, pp. 38-48, (2013).
- [30] Landes, J. D., and Begley, J. A., “The Effect of Specimen Geometry on J_{IC} ”, *American Society for Testing and Materials (ASTM STP 514)*, Vol. 10, pp. 24-29, (1972).
- [31] Marandet, B., and Sanz, G., “Evaluation of the Toughness of Thick Medium-strength Steels by using Linear-elastic Fracture Mechanics and Correlations Between K_{IC} and Charpy V-notch”, *Flaw Growth and Fracture (ASTM STP 631)*, Vol. 10, pp. 121-132, (1977).
- [32] Pense, A. W., and Stout, R. D., “*Fracture Toughness and Related Characteristics of the Steels*”, 4th Edition, WRC Bulletin, New York, (1975).
- [33] Rezayi-Yekta, M., “Computer Simulation of Grooved Sample from API X65 Steel with Gerson Model”, MSc. Thesis, Department of Mechanical Engineering, Birjand University, Birjand, Iran, (1389).
- [34] Rothwell, A. B., “Fracture Propagation Control for Gas Pipelines”, *Past, Present and Future Pipeline Technology*, Vol. 1, pp. 386-397, (2000).
- [35] Su, J. Q., Nelson, T. W., Mishra, R., and Mahoney, M., “Friction Stir Processing of 7075 Al Alloy and Subsequent Aging Treatment”, *Acta Materials*, Vol. 51, pp. 713-729, (1970).
- [36] Wallin, K., “The Scatter in K_{IC} -results”, *Engineering Fracture Mechanics*, Vol. 19, pp. 1085- 1093, (1984).
- [37] Wallin, K., “The Size Effect on K_{IC} -results”, *Engineering Fracture Mechanics*, Vol. 22, pp. 149-163, (1985).
- [38] Wallin, K., and Lee, S. T., “Fracture Toughness Transition Curve Shape for Ferritic Structural Steels”, *Fracture of Engineering Materials and Structures*, Vol. 42, pp. 83-88, (1991).
- [39] Zerbst, U., Ainsworth, R. A., Beier, H. T., and Pisarsk, H., “Review on Fracture and Crack Propagation in Weldments—A Fracture Mechanics Perspective”, *Engineering Fracture Mechanics*, Vol. 132, pp. 200-276, (2014).
- [40] ABAQUS Version 6.4 User’s Manual, (2005).
- [41] Marsavina, M., Linul, E., Voiconi, T, and Sadowski, T. A., “Comparison Between Dynamic and Static Fracture Toughness of Polyurethane Foams”, *Polymer Testing*, Vol. 4, pp. 131-132, (2013).

Nomenclatures

CT	: Compact Testing
CVN	: Charpy V-Notch
FSP	: Friction Stir Processing
BM	: Base-Metal
FS	: FSPed-Sample
FN5	: FSP Nano-ZrO ₂ -coated/560 rpm rotational speed
FN9	: FSP Nano-ZrO ₂ -coated/900 rpm
LEFM	: Linear Elastic Fracture Mechanics
K _{IC}	: Fracture Toughness
P _f	: Cumulative Failure Probability
T	: Temperature
A	: Area
J _{el}	: Elastic J Integral
J _{pl}	: Plastic J Integral

Greek Symbols

η	: Fracture Toughness Constant
--------	-------------------------------

چکیده

در این مقاله، تأثیر فرآیند اصطکاک اغتشاشی بر روی چقرمگی شکست فلز پایه St 37، مورد بررسی قرار گرفته است؛ در عین حال، تأثیر استفاده از نانو ذرات و تغییر سرعت دورانی فرآیند اصطکاک اغتشاشی بر روی نتیجه چقرمگی بررسی گردیده است. پس از انجام فرآیند در ۳ حالت متفاوت بدون نانو ذره، با نانو ذره و سرعت دورانی ۹۰۰ دور بر دقیقه، با نانو ذره با سرعت دورانی ۵۰۰ دور بر دقیقه؛ نتایج اندازه چقرمگی شکست از طریق آزمایش‌های شارپی و تست فشردگی استخراج و گزارش گردید. نتایج نشان دادند که انجام فرآیند و استفاده همزمان از نانو ذره با سرعت دورانی بالاتر بهترین عملکرد را دارد. این نتایج از هر دو آزمایش شارپی و تست فشردگی مورد صحت سنجی قرار گرفتند. در نهایت نتایج آزمایش‌ها با مدل سازی نرم افزاری انطباق داده شد و نتایج با یکدیگر مقایسه گردیدند.